

# International Conference on Space Optics—ICSO 2018

Chania, Greece

9–12 October 2018

*Edited by Zoran Sodnik, Nikos Karafolas, and Bruno Cugny*



## *Feasibility of a non-redundant pupil mask for in-flight wavelength measurements*

*Nicola Baccichet*

*Lucas Labadie*



ics0 proceedings



## Feasibility of a non-redundant pupil mask for in-flight wavelength measurements

Nicola Baccichet<sup>\*a</sup>, Lucas Labadie<sup>a</sup>

<sup>a</sup>I. Physikalisches Institut, Universität zu Köln, Zùlpicher Straße 77, 50937 Köln, Germany

### ABSTRACT

The study of sparse aperture masking as a mean to extract spectral information is a relatively little investigated content. However, despite the loss of throughput that comes with this technique, it allows one to benefit from the many advantages brought by interferometry, without the need of complex phase-controlled systems.

In this paper, we analyse the potential of non-redundant aperture masking for spectral measurements, highlighting its capabilities both as a tool for precise single-wavelength metrology, and as alternative to low resolution spectrographs.

Although here presented as a general introduction, this technique is suitable for a large number of potential applications, ranging from compact cube-sat missions for the analysis of bright sources, to large-dish space telescopes where the increased sensitivity allows one to study fainter targets.

**Keywords:** wavelength calibration, sparse aperture masking, interferometry, spectroscopy, SAM

### 1. INTRODUCTION

Sparse aperture masking (SAM) has been successfully employed in many space and ground-based optical instruments (e.g. [1]), where it can be embedded in a relatively straightforward way due to its inherent compactness, allowing a number of interferometric techniques to be exploited in a relatively inexpensive way. A prominent example is given by NIRISS, the near-IR instrument on board the James Webb Space Telescope, where a non-redundant array of apertures can be used to both co-phase the primary's mirror segments [2] and carry out high contrast imaging measurements of astronomical objects at a  $\lambda/2D$  angular resolution. In addition, the absence of atmospheric distortions means that fringe phase and amplitude can be easily measured in the interferogram produced by this pupil mask. Despite its success as an interferometric imaging tool, the possibility of extracting spectral information from SAM measurements has been less investigated so far. This is due to the low throughput that is characteristic of this masking technique, which makes detecting and separating individual spectral features more challenging. An alternative is pupil re-mapping [3] that is however, more difficult to implement compared to pupil-masking.

In this paper we analyse how SAM can be exploited from a spectral point of view, highlighting its potential both as internal metrology reference, as well as tool for surveying specific low-resolution spectral features of unresolved point sources. By coupling the ability of a non-redundant mask to sample specific spatial frequencies with the  $\lambda/B$  dependency of the spectrum, SAM can become particularly useful in carrying out repeated measurements for variability studies. In addition, as this information would be obtained directly at the instrument's focal plane, it becomes straightforward to take advantage of the Fourier power theorem to compensate for the loss in intensity. The simplicity of its implementation, allows also for easier hardware requirements and can virtually be included at zero costs within more complex systems with an accessible pupil.

Through simple software simulations, we illustrate what are the performance levels that can be reached when measuring the discrete spectral properties of an object, when using a non-redundant set of apertures placed in the pupil plane of a simple telescope. After that, we address the main challenges of its experimental feasibility with a laboratory test where we measure the interferograms generated by an extended object with multiple spectral lines.

\*baccichet@ph1.uni-koeln.de

## 2. PERFORMANCE STUDY

### 2.1 Theoretical background

The principle of this technique lies in the filtering properties that come naturally when considering Fourier optics: by acting selectively on the spatial transmission of the pupil of an optical system, specific patterns on the image plane can be analysed. In this way one can, for example, increase the spatial resolution below the classical diffraction limit and resolve objects at a  $\lambda/2D$  resolution – as it is nowadays the case in high contrast imaging observations in astronomy.

Another known property of interferometric systems, is the correlation between spectral power density and the distribution of illumination in the focal plane, which enables widely used techniques such as Fourier transform spectroscopy [4, 5]. This correlation can be also observed in light-gathering systems made of sparsely distributed apertures, by means of the wavelength dependence of its uv coverage, as a result of the following relation:

$$u_k = \pm \frac{x_i - x_j}{\lambda s}$$
$$v_k = \pm \frac{y_i - y_j}{\lambda s}$$

Where  $u_k, v_k$  represents a pair of uv coordinates,  $x_{i,j}, y_{i,j}$  are the coordinate pair (baselines) of two of the interferometer's apertures and  $s$  represents the propagation length. In case of focal plane interferometers, in the Fourier transform of the speckle pattern recorded by the detector array one can observe that each baseline appears in the form of a pattern of peaks radially distributed around the center. This is conceptually represented in Figure 1, where the uv coverage of a 6-apertures interferometer is shown as a function of wavelength, where all the different streaks contains both spectral and spatial information on the source being observed. This property consequently appears also when using a Sparse Aperture Mask (SAM), for which instrument concepts exist of combining its capabilities with additional means of separating wavelengths (e.g. IFU or grating) [6-8] in order to create a complete  $(x,y,\lambda)$  data cube. To achieve this, a complex set of hardware and advanced light-analysing elements is usually employed.

On the other hand, the performance and limitations of SAM used individually (i.e. only with simple focussing optics) have been little analysed quantitatively (to the author's knowledge), when used for spectral measurements. Nevertheless, due to its intrinsic stability (no moving elements) and simplicity, it can in principle allow easy access to spectral analysis almost for free, in any optical instrument having an accessible pupil.

Given that the interferogram pattern is fixed by internal alignment, the resulting peak positions are also fixed, thus facilitating the in-situ treatment of its images, aided also by the increase in sensitivity that arise when operating in Fourier space (power theorem). In addition, and contrarily to coating-dependent optical elements (e.g. immersed gratings), its spectral behaviour is inherently broadband and virtually aberration-free. Therefore, the same mask can operate across the full range permitted by the detector itself. By tuning the single aperture's size and detector's pixel density, one can create either a survey-like system operating at low spectral resolution or an instrument for analysing specific objects both spectrally and spatially [9-10]. Nevertheless, since throughput and spectral resolution are inversely related, one should tailor the shape of a SAM mask to gain the most advantage from these observation modes.

In order to provide a quantitative estimate of the performance one can expect, we make in the chapter that follows, a comparison between a double-apertures system and a 6-apertures one, having both the same filled diameter. In particular, we analyse through simulations, what is the spectral resolution and sensitivity that one can expect for different layouts, when observing a single, unresolved source.

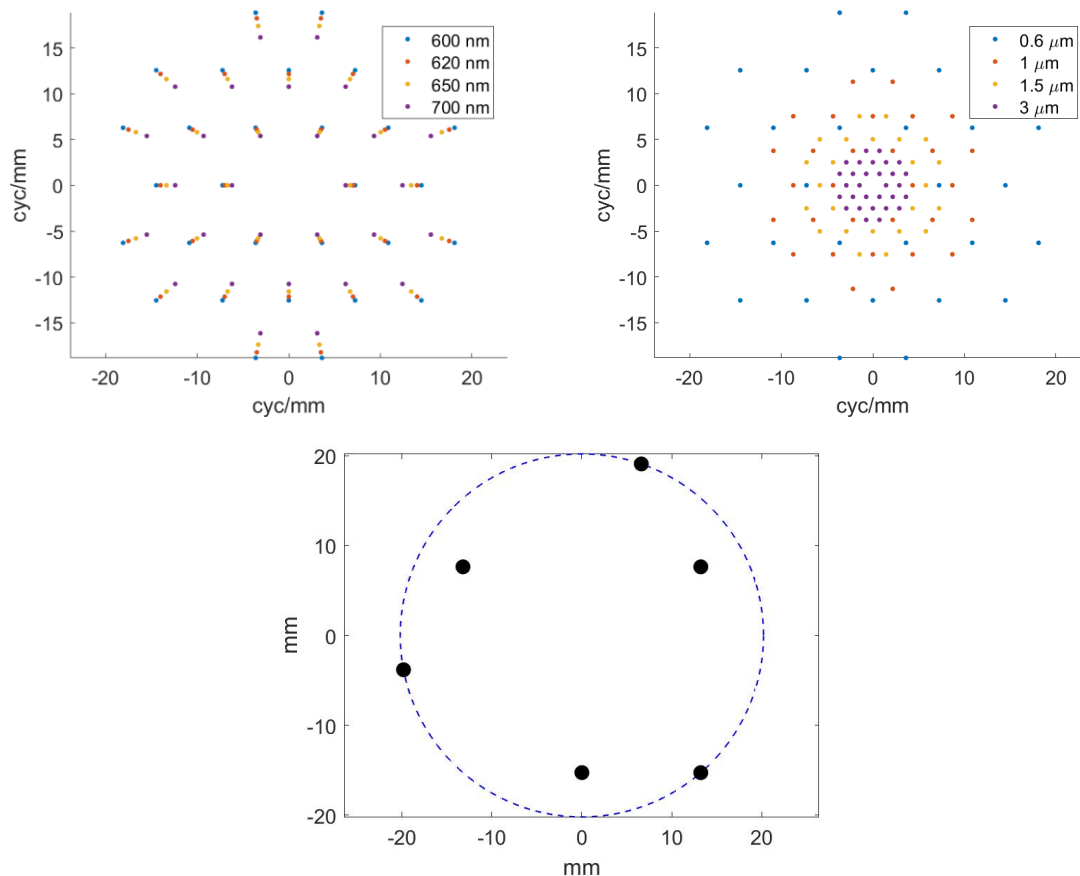


Figure 1: **(Top)** Illustrations of the uv coverage resulting from a six, non-redundant aperture mask, at different wavelengths. In these pictures, the generating mask has a maximum baseline of ~6cm. The figure on the left shows the distribution of light within a narrowband regime (visible), while on the right a larger wavelength range is considered. In both cases the dots are only representative of the uv points and do not correspond to a physical size; the central dot has been removed for clarity. **(Bottom)** Plot showing the mask layout where the dashed line represent the equivalent filled diameter [11].

## 2.2 Performance of a spectral SAM

To evaluate the performance that can be reached in spectral measurements with a SAM, we carried out several simulations of a simple optical instrument containing a masked pupil. In particular, we consider a small-sized optical system operating in space at infrared wavelengths (LM bands, ~3-5μm) with the specifications listed in Table 1. The reason for choosing a relatively compact system for these initial estimates, is the interest in focussing on some of the unique advantages that SAM can bring in term of stability and simplicity of the design.

As one can see from the parameters of Table 1, simulations are run considering different aperture sizes, ranging from 1mm to 10mm, in order to evaluate the relation between throughput and spectral resolution. In addition, to provide a more direct mean of comparison, the same analysis is carried out for both a six and- a two-apertures mask, when only an unresolved target is being observed within the instrument field of view.

Each simulations set is composed by a number of monochromatic focal plane images of consecutive wavelengths, defined by a given spectral resolution, in the range between 5 and 5000 and centred at 4.56μm. The complete sets are then build by varying the size of the individual apertures for both the two and six-apertures masks.

Using this simulated data, we initially run a calibration script that searches for the position of the uv peaks and determines the corresponding wavelength, based on the known geometrical properties of the system. In this way, we can quantify what is the accuracy with which a single line profile can be determined (i.e. calibration accuracy).

Subsequently, we create a polychromatic image by merging the individual focal plane interferograms. The result is then Fourier transformed to allow us inspecting the resulting fringe pattern and determine whether the group of individual lines can still be identified, thus determining the effective spectral resolution the system.

Table 1: Parameters of the sparse-aperture masked optical system adopted in the simulations.

Parameter	Value(s)
Entrance pupil diameter	70mm
Focal length	0.5m
Detector size	2048x2048
Center wavelength	4.65 $\mu\text{m}$
Spectral resolutions (R)	5, 10, 30, 50, 80, 100, 1000, 5000
Pixel size	18 $\mu\text{m}$
Largest apertures baseline	55 mm
Size of individual apertures	1, 2, 4, 10 mm
Number of apertures	2 or 6

### 2.2.1 Simulations analysis

To quantify the performance expected from each mask, we consider three parameters: the precision with which each individual wavelength can be identified (calibration accuracy), the spectral resolution at which lines can be resolved and the relative throughput in comparison to the corresponding filled aperture of the system. Figure 2 shows the 3D distribution of these parameters for each mask configuration, where the blue points refer to the 6-apertures mask and the red ones to the 2-apertures one.

As one can see, we find that single wavelength calibration is in general more accurate with a six-apertures system since more uv points (i.e. detector area) can be used to unequivocally determine the wavelength of the light, as well as providing more throughput and brighter peaks. On average we find that one can reach  $R \sim 10\,000$  with this system, compared to a smaller  $R \sim 2000$  obtained on average with a two apertures mask.

When looking instead at the spectral resolving power, we noticed that both systems allow the clear identification of individual lines up to circa  $R=100$ , where the single peaks could be clearly identified. At higher resolutions the peaks start blending into more uniform streaks, but thanks to the higher calibration accuracy provided by considering the individual lines, the position of the peaks could be identified also for  $R=1000$ . At  $R=5000$  instead both systems could be calibrated but lines were fully blended in the polychromatic image.

Throughput wise, it appears clear that the 6-apertures mask allows fainter targets to be observed. Nevertheless, due to the larger uv area covered, line blends already at  $R=100$  when considering the largest single-aperture diameter, which can still be identified thanks to the pixel-to-wavelength calibration that provides subpixel accuracy. This can be further mitigated by considering a smaller single-aperture diameter in fact, as one can see from the highest peaks of Figure 2 the increased number of holes can compensate for the line blending and still provide higher throughput for an equal spectral resolution.

Overall, simulations show that both the six- and two-apertures mask allow spectral measurements up to  $R=1000$  at  $4.56\mu\text{m}$ , with the 6-apertures one providing the higher throughput and wavelength-to-pixel accuracy.

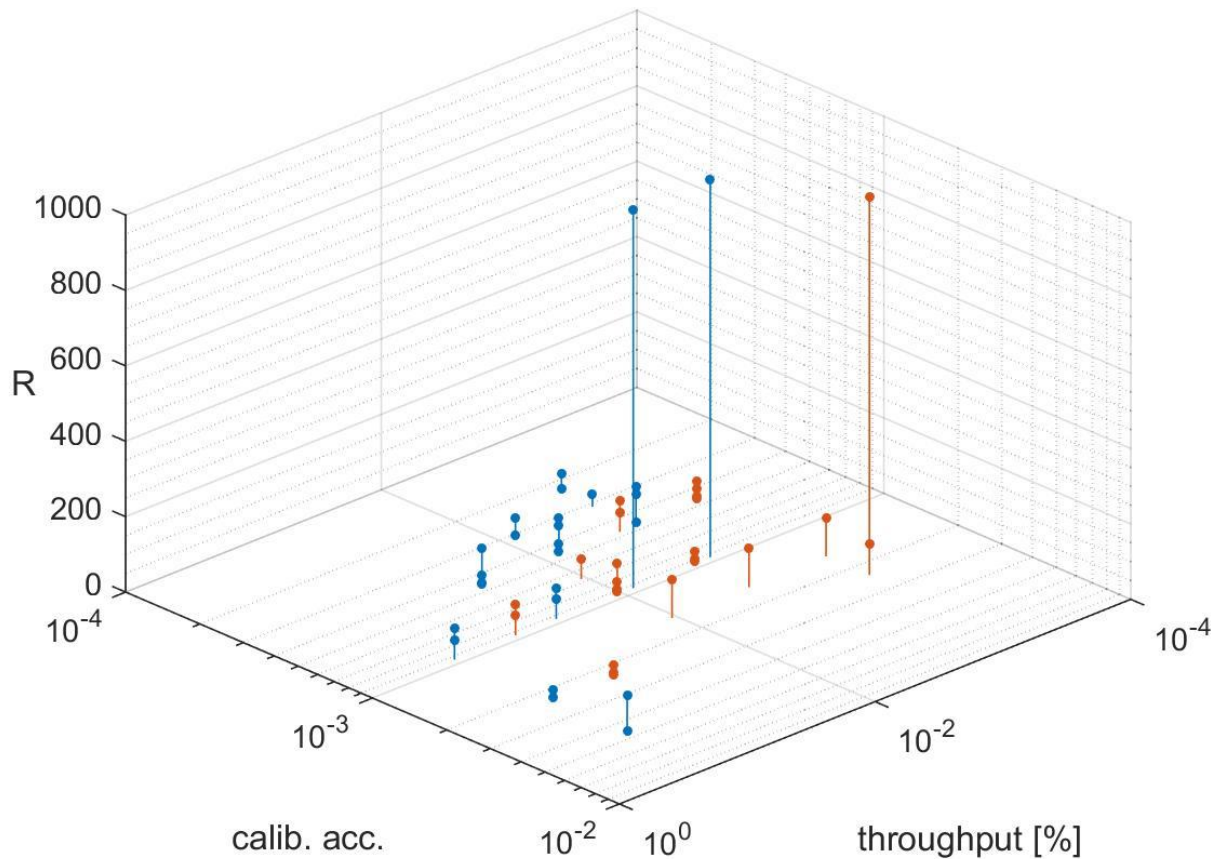


Figure 2: 3D plot illustrating the spectral performance of a two- and a six-aperture masked optical instrument, when observing an unresolved source. The blue lines refer to the six-aperture simulations, while the red ones to the two-aperture data. R and the calibration accuracy have been calculated at the center wavelength of  $4.56\mu\text{m}$ .

### 3. LABORATORY MEASUREMENTS

To validate the calibration technique used in the previous section and investigate what realistically one can expect from an actual spectral SAM, we made a simple laboratory measurement of a 6-apertures non-redundant pupil mask using several sources. At this stage, focus was given to ease of alignment and system verification, therefore the choice of observing in the visible wavelength range.

Figure 3 shows the system in its core elements: light is injected either through a fiber or from an alignment laser into a double beam expander, which enlarges the beam before it impinges onto a 1-inch pupil mask, made of six holes  $300\mu\text{m}$  in diameter and with maximum baseline of 10mm. The light sources consist on two lasers at 635nm and 632.8nm, as well as a fiber-fed Krypton lamp, which can be swapped with the fibered output of the HeNe laser (632.8nm). Spatial filters and baffles (not shown in the picture) help reducing the straylight that arrives onto the detector: an off-the-shelf 1-megapixel CCD, with pixels pitch of  $3.5\mu\text{m}$  and 8bit dynamic range (placed  $\sim 0.5\text{m}$  away from focussing lens and not shown in Figure 3).

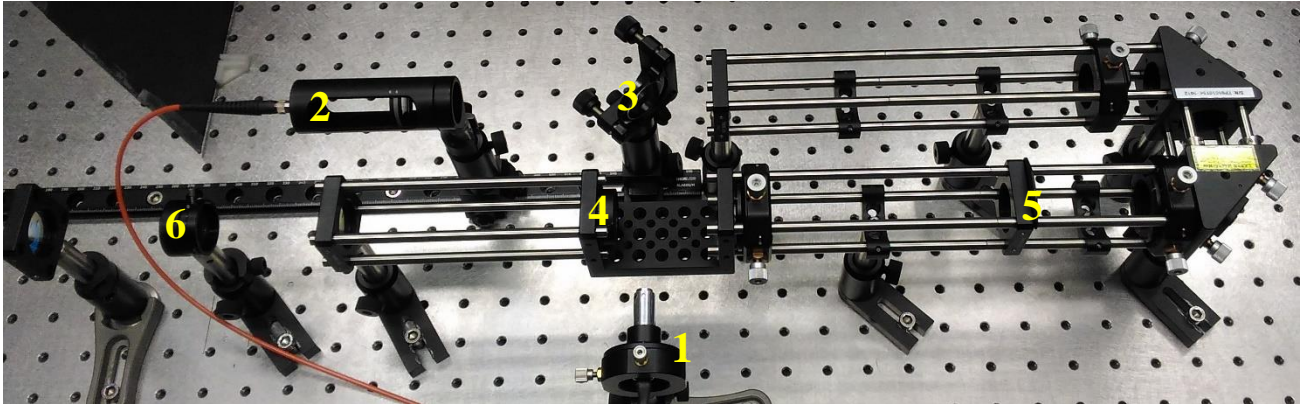


Figure 3: Picture of the laboratory setup used to analyse the spectral resolving power of a 6-apertures non redundant pupil mask. 1: 635nm calibration laser; 2: output of fiber sources (Kr lamp and 632.8nm HeNe laser – not shown); 3: pellicle beam splitter feeding the light into a double beam expander; 4: pupil mask; 5,6: spatial filters. The detector is located  $\sim 0.5\text{m}$  on the left from the last lens of the system.

### 3.1 Calibration

Before analysing the data acquired from this setup, all images were flat and dark corrected and after that, stacked in order to increase the signal-to-noise provided by each individual frame.

At first, we used the 635nm laser to calibrate the system and determine with precision its focal length. To do so, its interferogram was Fourier transformed and basing on the location of the uv peaks (visibilities) and laser wavelength, the remaining geometrical parameters could be fixed. Figure 4 shows the result of this procedure, where the positions of the peaks return an equivalent focal length of about 600mm.

After that, to verify the validity of this measurement, we used the so-found length to determine the peaks position of the HeNe laser, emitting at 632.8nm. In this case, the peaks location fall well within the prediction but no noticeable difference between the 635nm uv peaks could be found, indicating that the instrument resolving power is lower than what needed to identify the two lines, which is  $R \sim 300$  at 635nm.

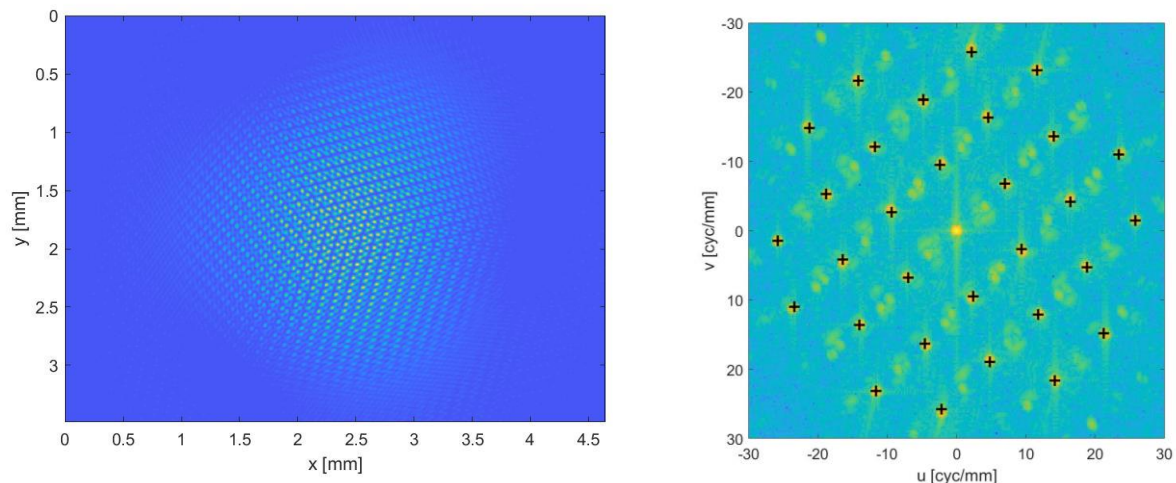


Figure 4: **(Left)** detector image showing the interferometric pattern produced by the 6-apertures mask for the 635nm laser. **(Right)** Fourier transformed image showing the resulting uv coverage with overlapped the points found after calibration (black crosses). Some sources of noise (possibly straylight) can be identified but are 2 orders of magnitude lower intensity compared to the uv peaks formed by the laser and can be discarded from the analysis.

### 3.2 Analysis of the spectrum of Kr

To assess the polychromatic behaviour of the system's SAM, a fiber-fed Krypton lamp was used. In this case, given its low brightness compared to the two lasers, about 2000 individual frames were stacked in order to produce a detectable signal, which can be seen on the left side of Figure 5. Here one can see that instead of peaks the Fourier-transformed image shows elongated streaks, corresponding to the brightest emission lines of Krypton, which lie between 750 and 900nm.

By using the calibration data obtained with the laser sources and referring to the known emission spectrum of the lamp, we were able to overlap on the image the brightest lines expected to emit in the visible range. As one can see from the left side of Figure 5, the peaks position could approximately be identified but without being able to resolve the individual lines. By observing the light distribution of the image, we were able to identify the blended emission of the lines around 820nm and 880nm, the distance of which indicates that the spectral resolution of the system in use is  $R \sim 3$  in this wavelength range.

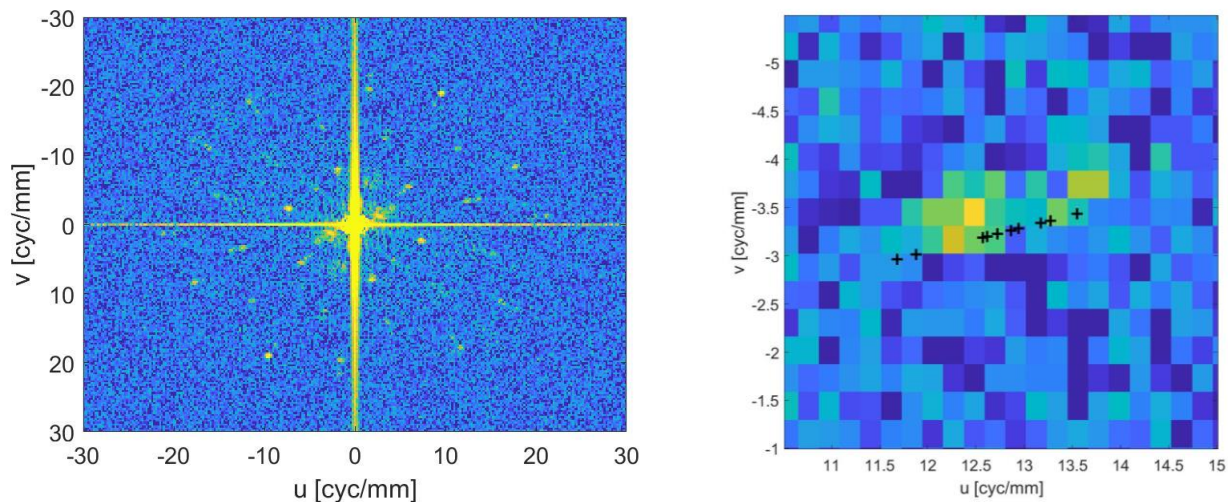


Figure 5: **(Left)** Fourier transform of the focal plane image obtained when observing the Krypton lamp. The color scale has been stretched to better highlight the uv points. **(Right)** zoomed image of one uv streak with superimposed the predicted position of the major emission lines of Krypton, in the region between 750nm (outer points – right side) and 900nm (inner points – left side). The brightest pixels correspond to the blended lines lying around 820nm.

## 4. CONCLUSIONS

In this paper we have analysed on a high-level, what are the performance to be expected when using a sparse-aperture pupil mask to carry out spectral measurements. Through simple simulations of a conceptual instrument, we have shown that SAM can constitute a valid alternative to, for example, a classic double-slit spectrograph since it allows for a higher throughput and calibration accuracy (provided that both are used in the same optical configuration). Clear advantages that such a mask would bring are: its inherent broadband behaviour, which can even span across wavelength regimes (VIS, IR); the simplicity in terms of hardware requirements for its implementation and the relative compactness required for it to operate. Thanks to the larger detector area that SAM can make use of, a subpixel accuracy in wavelength calibration can be achieved, allowing one to disentangle even blended features and compensate for the loss in throughput required for the pupil mask to function. Overall we were able to show that a 6-apertures mask can deliver up to  $R=1000$  at  $4.56\mu\text{m}$ , with a wavelength-to-pixel calibration accuracy of  $10^{-4}$ .

With these characteristics a spectral SAM could be included in a relatively straightforward manner in the pupil plane of a large telescope, functioning either as a precise wavelength calibration tool or to carry out quick spectral diagnostics of spatially known sources. Alternatively, given the small size required for it to work, it could be implemented in a CubeSat system or a swarm of, to carry out variability studies of bright objects. In future work, an exhaustive analysis of  $R$  vs throughput will allow us to define a more complete set of use cases and corresponding performance, for spectroscopy with a non-redundant pupil mask.

Moreover, we were able to validate through laboratory measurements the wavelength calibration procedure, showing that it matches well the prediction for both laser sources employed, although the system did not allow the spectral resolution needed to clearly separate both lines. Nevertheless, with the calibrated data we were able to predict the position of the Krypton visible lines, which could be identified in two blended uv streaks, regardless of the faint emission of the lamp. Future work will include the increase of the resolution of this setup in order to reach  $R=300$  at 600nm, allowing us to resolve both the lasers and Krypton lines and possibly investigate, from a practical point of view, what are the limitations of such a system in providing also image reconstruction capabilities.

## REFERENCES

- [1] Tuthill, P. G. et al., “Sparse aperture masking (SAM) at NAOS/CONICA on the VLT” in *Proceedings of the SPIE*, Volume 7735, id. 77351O (2010).
- [2] Sivaramakrishnan, A. et al., “Non-redundant Aperture Masking Interferometry (AMI) and segment phasing with JWST-NIRISS” in *Space Telescopes and Instrumentation 2012: Optical, Infrared, and Millimeter Wave. Proceedings of the SPIE*, Volume 8442, article id. 84422S, 14 pp. (2012).
- [3] Perrin, G., Lacour, S., Woillez, J., & Thiebaut, E. “High dynamic range imaging by pupil single-mode filtering and remapping” *Monthly Notices of the Royal Astronomical Society*, 373(2), 747–751 (2006).
- [4] Itoh, K., & Ohtsuka, Y. “Fourier-transform spectral imaging: retrieval of source information from three-dimensional spatial coherence” *Journal of the Optical Society of America A*, 3(1), 94 (1986).
- [5] Born, M., & Wolf, E. (1999). *Principles of Optics* (7th ed.). Cambridge University Press.
- [6] Matsuo, T., Itoh, S., Shibai, H., Sumi, T., & Yamamuro, T. “A NEW CONCEPT FOR SPECTROPHOTOMETRY OF EXOPLANETS WITH SPACE-BORNE TELESCOPES” *The Astrophysical Journal*, 823(2), 139 (2016).
- [7] Itoh, S., Matsuo, T., Goda, S., Shibai, H., & Sumi, T. “Pupil Masks for Spectrophotometry of Transiting Exoplanets” *The Astronomical Journal*, 154(3), 97 (2017).
- [8] Brandl B. et al. “Status of the Mid-IR ELT Imager and Spectrograph METIS” in *SPIE 10702 Astronomical Telescopes & Instrumentation* (2018).
- [9] Dohlen, K., Vives, S., Rakotonimbahy, E., Sarkar, T., Tasnim Ava, T., Baccichet, N., Swinyard, B. “Design of a nano-satellite demonstrator of an infrared imaging space interferometer: the HyperCube” In *SPIE 9146, Optical and Infrared Interferometry IV* (Vol. 9146, p. 914603) (2014).
- [10] Baccichet, N., Caillat, A., Rakotonimbahy, E., Dohlen, K., & Savini, G. “Ground results from a space-based Fizeau interferometer demonstrator” In *Far Infrared Space Interferometer Critical Assessment – 3rd Workshop: Bringing Far Infrared Interferometry Into Vision* (pp. 1–7) (2015).
- [11] Golay, M. J. E. “Point Arrays Having Compact, Nonredundant Autocorrelations” *Journal of the Optical Society of America*, 61, 272–273 (1970).